AMERICAN JOURNAL OF PHYSIOLOGY
RENAL PHYSIOLOGY

Am J Physiol Renal Physiol 321: F455–F465, 2021.
First published August 23, 2021; doi:10.1152/ajprenal.00111.2021

RESEARCH ARTICLE

Antibiotic-induced microbiome depletion alters renal glucose metabolism and exacerbates renal injury after ischemia-reperfusion injury in mice

Yuika Osada, Shunsaku Nakagawa, Kanako Ishibe, Shota Takao, Aimi Shimazaki, Kotaro Itohara, Satoshi Imai, Atsushi Yonezawa, Takayuki Nakagawa, and Kazuo Matsubara

Department of Clinical Pharmacology and Therapeutics, Kyoto University Hospital, Kyoto, Japan

Abstract

Recent studies have revealed the impact of antibiotic-induced microbiome depletion (AIMD) on host glucose homeostasis. The kidney has a critical role in systemic glucose homeostasis; however, information regarding the association between AIMD and renal glucose metabolism remains limited. Hence, we aimed to determine the effects of AIMD on renal glucose metabolism by inducing gut microbiome depletion using an antibiotic cocktail (ABX) composed of ampicillin, vancomycin, and levofloxacin in mice. The results showed that bacterial 16s rRNA expression, luminal concentrations of short-chain fatty acids and bile acids, and plasma glucose levels were significantly lower in ABX-treated mice than in vehicle-treated mice. In addition, ABX treatment significantly reduced renal glucose and pyruvate levels. mRNA expression levels of glucose-6-phosphatase and phosphoenolpyruvate carboxykinase in the renal cortex were significantly higher in ABX-treated mice than in vehicle-treated mice. We further examined the impact of AIMD on the altered metabolic status in mice after ischemia-induced kidney injury. After exposure to ischemia for 60 min, renal pyruvate concentrations were significantly lower in ABX-treated mice than in vehicle-treated mice. ABX treatment caused a more severe tubular injury after ischemia-reperfusion. Our findings confirm that AIMD is associated with decreased pyruvate levels in the kidney, which may have been caused by the activation of renal gluconeogenesis. Thus, we hypothesized that AIMD would increase the vulnerability of the kidney to ischemia-reperfusion injury.

NEW & NOTEWORTHY This study aimed to determine the impact of antibiotic-induced microbiome depletion (AIMD) on renal glucose metabolism in mice. This is the first report confirming that AIMD is associated with decreased levels of pyruvate, a key intermediate in glucose metabolism, which may have been caused by activation of renal gluconeogenesis. We hypothesized that AIMD can increase the susceptibility of the kidney to ischemia-reperfusion injury.

gluconeogenesis; ischemia; lactate; metabolic remodeling; pyruvate

INTRODUCTION

Antibiotics are widely used for the prevention and treatment of infectious diseases. Possessing bactericidal or bacteriostatic activity against both pathogenic and commensal bacteria, antibiotics can directly affect the gut microbiome composition (1, 2). It has been known that patients admitted to intensive care units are often treated with multiple antibiotics and that they have altered gut microbiota (3, 4), suggesting that antibiotic use could affect the diversity and number of gut microbiota in patients (5, 6). Therefore, understanding the effects of antibiotic-induced reduction of gut microbiota on host physiology and organ homeostasis is vital.

Since intestinal bacteria produce short-chain fatty acids (SCFAs) and bile acids, a decrease in gut microbiome abundance leads to a reduction in the luminal contents of SCFAs and bile acids in the intestinal tract (7–9). Recent studies have revealed an association between antibiotic-induced microbiome depletion (AIMD) and changes in host glucose homeostasis (10, 11). Zarrinpar et al. (11) reported that AIMD enhances anaerobic glycolysis in cecal epithelial cells of mice and upregulates the expression of genes coding for key enzymes involved in hepatic gluconeogenesis, specifically glucose-6-phosphatase (*G6pc*) and pyruvate carboxylase (*Pcx*), suggesting an association between AIMD and enhanced gluconeogenesis in the mouse liver.

The kidney has a distinctive role in glucose homeostasis by modulating not only glucose utilization but also gluconeogenesis and glucose reabsorption from renal tubules (12). This organ is responsible for up to 20% of endogenous glucose production via gluconeogenesis (13) and has the capacity for lactate uptake and pyruvate release, thereby maintaining pyruvate and lactate levels in the blood (14). However, despite the critical role of the kidney in systemic glucose homeostasis, information regarding the effect of AIMD on renal glucose metabolism remains limited.

Renal glucose metabolism is affected by multiple factors, including nutritional status and renal and extrarenal diseases (15–18). A previous study revealed the rapid changes in

Correspondence: S. Nakagawa (nakashun@kuhp.kyoto-u.ac.jp).
Submitted 19 March 2021 / Revised 13 August 2021 / Accepted 13 August 2021

the renal contents of glucose and its metabolites (pyruvate and lactate) after exposure to ischemia and glycerol-induced kidney injury (19). Likewise, Smith et al. (20) reported decreased renal pyruvate levels in mouse kidneys after lipopolysaccharide-induced acute kidney injury (AKI). Given the impact of AKI on renal glucose metabolism, the effect of AIMD on metabolic status in the kidneys during ischemia requires elucidation.

Hence, we aimed here to determine the impact of AIMD on renal glucose metabolism in mice. To test this, we quantified renal glucose metabolites in mice treated with broad-spectrum antibiotics and later subjected to renal ischemia. Our findings may provide new insights regarding the effects of AIMD on renal glucose metabolism.

MATERIALS AND METHODS

Chemicals and Reagents

Sterilized and analytical grade reagents and chemicals were obtained as described below. PBS, ampicillin, vancomycin, levofloxacin, ethyl Carnoy's solution, 4% paraformaldehyde in PBS, glucose, acetate, propionate, butyrate, ursodeoxycholate, pyruvate, lactate, benzoate, 3-nitrophenylhydrazine, pyridine, acetyl-CoA, acetonitrile, ultrapure water, formic acid, ammonium acetate, K_2CO_3, and 4′,6-diamidino-2-phenylindole were purchased from Wako Pure Chemical Industries (Osaka, Japan). Cholate, deoxycholate, citrate, α-ketoglutarate, succinate, fumarate, malate, ATP, $HClO_4$, BSA, and Triton X-100 were purchased from Nacalai Tesque (Kyoto, Japan). *N*-(3-dimethylaminopropyl)-*N*′-ethylcarbodiimide and optimal cutting temperature (OCT) compound were obtained from Sigma-Aldrich (St. Louis, MO) and Sakura Fine Technical (Tokyo, Japan), respectively.

Animals

Consistent with most previous studies investigating the effects of AIMD on systemic metabolism (9–11, 21–24), only male mice were used in this study. Male BALB/c mice (8 wk old) were obtained from SLC Animal Research Laboratories (Shizuoka, Japan) and maintained in accordance with the Guidelines for Animal Experiments of Kyoto University (Kyoto, Japan). All protocols were approved by the Animal Research Committee of the Graduate School of Medicine, Kyoto University (Permit No. Medkyo 20122). Mice were housed in a specific pathogen-free facility, kept in a temperature-controlled environment with a 12:12-h light-dark cycle, and received a standard diet and water ad libitum. For commensal depletion, mice were administered with an antibiotic cocktail (ABX) via drinking water for 3, 7, 10, or 14 days. ABX was composed of 1 g/L ampicillin, 0.5 g/L vancomycin, and 0.5 g/L levofloxacin and was dissolved in sterilized water. Control mice received vehicle (sterilized water) only.

At the end of each experiment, mice were euthanized under isoflurane-induced anesthesia, and the plasma, colon, and kidneys were collected. The luminal content of the colon was removed by flushing with sterile PBS and gently squeezing out the intestinal content into a collection tube. The plasma, intestinal and colon luminal content, whole kidney, and dissected kidney showing the cortex were rapidly frozen in liquid nitrogen and stored at −80°C. For pathological evaluation, resected kidneys were fixed in ethyl Carnoy's solution. To evaluate protein expression of kidney injury molecule-1 (Kim-1), mice were perfused with 4% paraformaldehyde in PBS, and the kidneys were dissected.

Quantification of Glucose and the Glucose Tolerance Test

The glucose tolerance test was performed on fasted mice (4 h) by monitoring plasma glucose levels. Briefly, mice were fasted for 4 h before an intraperitoneal injection with glucose (1 g/kg body wt). Glucose levels in the plasma and kidney were measured using a colorimetric assay (LabAssay Glucose, Wako Pure Chemical Industries) according to the manufacturer's protocol.

Renal Ischemia and Ischemia-Reperfusion

To evaluate the effect of renal ischemia on glucose metabolism, mice were subjected to ischemia-reperfusion (IR) after 14 days of treatment with ABX or vehicle (for the control). Mice were anesthetized (induced by medetomidine, midazolam, and butorphanol) and placed on a homeothermic table, and body temperature levels were monitored and maintained at 37°C during surgical procedures. For unilateral renal ischemia (60 min), mice were subjected to a midline abdominal incision, and the left renal pedicle was clamped with a nontraumatic clamp (Natsume Seisakusho, Osaka, Japan) for 60 min, followed by resection of the clamped and contralateral (control) kidneys. To induce IR injury, a back incision was made to expose the left renal pedicle. The left renal pedicle was clamped for 30 min, followed by 24 h of reperfusion. The back incision was closed with two layers of sutures, and mice recovered from anesthesia. The kidneys were resected after the reperfusion period.

Assessment of Microbiome Depletion

Microbiome depletion was assessed based on the relative expression levels of 16s rRNA in the colon luminal contents. Total DNA was extracted from samples using the NucleoSpin DNA Stool Mini Kit (Macherey-Nagel, Düren, Germany) according to the manufacturer's protocols. Quantitative PCR analysis was performed using Power SYBR Green PCR Master Mix (Applied Biosystems, ThermoFisher Scientific, Waltham, MA) and the StepOnePlus Real-Time PCR System (Applied Biosystems, ThermoFisher Scientific) according to the manufacturer's instructions. The following primers were used for amplification: 16s rDNA forward primer 5′-GGTGAATACGTTCCCGG-3′ and reverse primer 5′-TACGGCTACCTTGTTACGACTT-3′ (25). The relative quantity of 16s rDNA in the same amount of total DNA was calculated using the ΔC_t method (where C_t is the threshold cycle).

Quantification of SCFAs, Bile Acid, and Organic Acids

Acetate, propionate, butyrate, cholate, deoxycholate, ursodeoxycholate, pyruvate, lactate, citrate, α-ketoglutarate, succinate, fumarate, and malate were quantified as their 3-nitrophenylhydrazones using liquid chromatography-tandem mass spectrometry (LC-MS/MS) following previously published protocols (26–29). For organic acid extraction, the kidneys were homogenized in nine volumes of 50% acetonitrile (9 μL/1 mg tissue). A 50 μL standard solution (mixture of

acetate, propionate, butyrate, pyruvate, lactate, citrate, α-ketoglutarate, succinate, fumarate, and malate or mixture of cholate, deoxycholate, and ursodeoxycholate), intestinal contents, plasma, or homogenized kidney was added to 250 μL of 100 μM benzoate (internal standard) in 100% acetonitrile and centrifuged at room temperature for 10 min at 10,000 *g*. For derivatization, 40 μL of the supernatant was mixed with 20 μL of 200 mM 3-nitrophenylhydrazine in 50% aqueous acetonitrile and 20 μL of 120 mM *N*-(3-dimethylaminopropyl)-*N*′-ethylcarbodiimide-6% pyridine solution in the same solvent. The mixture was incubated at 40°C for 30 min and allowed to react. After the reaction, the solution was diluted with 2 mL of 10% aqueous acetonitrile. LC-MS/MS analysis was performed using the LCMS-8040 system (Shimadzu, Kyoto, Japan) set to multiple reaction monitoring mode in negative ion mode. Reversed-phase chromatography was performed on a COSMOSIL 5 C_{18}-MS-II column (4.6 × 150 mm, 5 μm, Nacalai Tesque). The mobile phase was composed of 0.1% formic acid in water (*A*) and 0.1% formic acid in acetonitrile (*B*). For analysis of SCFAs and organic acid, the gradient elution was performed as follows (flow rate at 0.35 mL/min): initial elution at 15% *B* for 1.0 min, followed by a linear increase to 55% *B* for 5.0 min, then 80% *B* for 1.5 min, with a hold at 80% *B* for 2.0 min, and then decreased linearly to 15% *B* for 1.5 min. For analysis of bile acid, the gradient elution was performed as follows (flow rate at 0.45 mL/min): initial elution at 30% *B* for 1.0 min, followed by a linear increase to 80% *B* for 3.0 min, then 91.7% *B* for 7.0 min, and then decreased linearly to 30% *B* for 0.5 min. The following ion transitions were monitored to detect each metabolite: acetate, from *m/z* 194.1 to 137.0; propionate, from *m/z* 207.9 to 137.0; butyrate, from *m/z* 222.1 to 137.0; cholate, from *m/z* 542.2 to 137.0; deoxycholate, from *m/z* 526.2 to 152.0; ursodeoxycholate, from *m/z* 526.1 to 137.1; pyruvate, from *m/z* 357.1 to 137.0; lactate, from *m/z* 224.1 to 137.0; citrate, from *m/z* 596.0 to 222.1; α-ketoglutarate, from *m/z* 550.0 to 233.1; succinate, from *m/z* 386.9 to 152.1; fumarate, from *m/z* 384.9 to 137.0; malate, from *m/z* 403.1 to 137.0; and benzoate, from *m/z* 255.9 to 137.0 (where *m/z* is the mass-to-charge ratio).

ELISA of Plasma Glucagon-Like Peptide 1 and Insulin

Plasma glucagon-like peptide 1 (GLP-1) and insulin levels were determined using GLP-1 ELISA (Wako Pure Chemical Industries) and LBIS Mouse Insulin ELISA (Shibayagi, Gunma, Japan) kits, respectively, according to the manufacturer's protocols.

Quantification of Acetyl-CoA and ATP

For the extraction of acetyl-CoA and ATP, the tissue was homogenized with nine volumes of 0.3 M $HClO_4$ (9 μL/1 mg tissue), incubated on ice for 10 min, and centrifuged at 10,000 *g* for 10 min. The supernatant (400 μL) was neutralized with 135 μL of 0.5 M K_2CO_3, and the precipitate was removed by centrifugation (at 4°C for 10 min at 14,000 *g*). The neutralized supernatants were subjected to LC-MS/MS analysis and reversed-phase chromatography following the methods described earlier. The mobile phase was composed of 1 mM ammonium acetate in water (*A*) and 1 mM ammonium acetate (*B*) in methanol. The gradient elution was programmed as follows (flow rate at 0.2 mL/min): initial elution with 2% *B* in 2.0 min, followed by a linear increase to 25% *B* in 3.5 min, then to 100% *B* in 0.5 min, held at 100% *B* in 4.0 min, and then decreased linearly to 2% *B* in 1.0 min. The ion transition from *m/z* 810.0 to 303.1 in positive ion mode was monitored to detect acetyl-CoA (30). ATP levels were quantified using a CellTiter-Glo luciferase/luciferin assay (Promega, Madison, WI) according to the manufacturer's instructions, and luminescence levels were measured using a LB 940 luminometer (Berthold, Bad Wildbad, Germany).

Quantitative RT-PCR

Total RNA was extracted from ~40 mg of mouse kidneys using the RNeasy Mini Kit (Qiagen, Hilden, Germany) and then reverse transcribed using a High-Capacity cDNA Reverse Transcription Kit (ThermoFisher Scientific). Quantitative RT-PCR was performed using the methods described earlier. Relative mRNA expression levels of target genes were calculated using the $2^{-\Delta\Delta Ct}$ method, with *Gapdh* as the reference. The following primer pairs were used for amplification (11, 20, 31–34): *Gapdh*, 5′-TGAACGGATTTGGCCGTATTGG-3′ and 5′-TGCCGTGAGTGGAGTCATACTG-3′; glucose transporter 1 (*Glut1*), 5′-AGATGAAAGAAGAGGGTCGG-3′ and 5′-AGAACACAGCATTGATACCC-3′; glucose transporter 2 (*Glut2*), 5′-TCCTCGTGGCGCTGATG-3′ and 5′-CTGGTTGAATAGTAAAATATCCCATTGAT-3′; Na^+-glucose cotransporter 1 (*Sglt1*), 5′-AAGATCCGGAAGAAGGCATC-3′ and 5′-CAATCAGCACGAGGATGAAC-3′; Na^+-glucose cotransporter 2 (*Sglt2*), 5′-TATTGGTGCAGCGATCAGG-3′ and 5′-CCCAGCTTTGATGTGAGTCAG-3′; *G6pc*, 5′-CAGTGGTCGGAGACTGGTTC-3′ and 5′-GTCCAGGACCCACCAATACG-3′; hexokinase 1 (*Hk1*), 5′-GGGACTATGACGCTAACATT-3′ and 5′-CCAGTGCCAATGATCAGG-3′; hexokinase 2 (*Hk2*), 5′-GGTACAGAGAAAGGAGACTTC-3′ and 5′-TCTTGTTATGCATCTCTACGC-3′; hexokinase 3 (*Hk3*), 5′-CACTTAACCAATCTCGGAGT-3′ and 5′-AGGCTATCACTTTCGATCTC-3′; fructose-bisphosphatase 1 (*Fbp1*), 5′-AGTCGTCCTACGCTACCTGTG-3′ and 5′-GGGGATCGAAACAGACAACAT-3′; *Pcx*, 5′-GTTCCGTGTCCGAGGTGTAA-3′ and 5′-AACTGGGTGTCCACTGTGC-3′; phosphoenolpyruvate carboxykinase 1 (*Pepck*), 5′-GAGATAGCGGCACAAT-3′ and 5′-TTCAGAGACTATGCGGTG-3′; lactate dehydrogenase A (*Ldha*), 5′-TGTCTCCAGCAAAGACTACTGT-3′ and 5′-GACTGTACTTGACAATGTTGGGA-3′; and lactate dehydrogenase B (*Ldhb*), 5′-CATTGCGTCCGTTGCAGATG-3′ and 5′-GGAGGAACAAGCTCCCGTG-3′.

Histological Staining and Evaluation

For periodic acid-Schiff (PAS) staining, the kidneys were fixed in ethyl Carnoy's solution for 24 h and subsequently transferred to 70% ethanol (35). Tissues were embedded in paraffin and stained with PAS (Sapporo General Pathology Laboratory, Sapporo, Japan). Histological evaluations were performed as previously described (36–38). Tubular injury was scored semiquantitatively by blinded evaluators who examined the PAS-stained kidney sections, with 10 and 5 fields of view (×200 magnification) for the cortex and outer stripe of the outer medulla (OSOM), respectively. Tubular injury was defined as tubular necrosis, tubular cast formation, or loss of the brush border. The tubular injury score in each mouse kidney was assessed on a scale of 0–5, where 0 = no tubular injury, 1 = ≤10% tubules injured, 2 = 10–25%

tubules injured, 3 = 25–50% tubules injured, 4 = 50–75% tubules injured, and 5 = ≥75% tubules injured.

To examine the degree of proximal tubule injury, Kim-1 expression was examined. The F-actin was stained with fluorescein phalloidin. The dissected kidneys were postfixed in 4% paraformaldehyde for 3 h and transferred to 30% sucrose in PBS overnight at 4°C. The kidneys were embedded in OCT compound and frozen in liquid nitrogen. The snap-frozen kidneys were cut into 5-μm-thick transverse sections using a freezing microtome (Leica, Tokyo, Japan). Sections were covered with 5% BSA containing 0.3% Triton X-100 at 37°C for 60 min and then subjected to immunofluorescence analysis. Subsequently, sections were incubated overnight at 4°C with Kim-1-specific primary antibody [previously developed in our laboratory (39), 1:200], washed three times with PBS, and incubated with Alexa Fluor 546-labeled goat anti-rabbit IgG (Life Technologies, Tokyo, Japan, 1:400), Alexa Fluor 488-phalloidin (Life Technologies, 1:400), and 4′,6-diamidino-2-phenylindole at 37°C for 60 min. Images were visualized and captured using a fluorescence microscope (BZ-9000, Keyence, Osaka, Japan) with its software (BZ-II Analyzer, Keyence). To evaluate protein levels of Kim-1, the stained area in each mouse kidney was quantified and expressed as a percentage of each section, according to previous studies (40, 41).

Statistical Analysis

Results are expressed as means ± SD. Statistical analysis was performed using GraphPad Prism version 8.0 software (GraphPad, San Diego, CA). The data were analyzed using an unpaired *t* test or multiple-comparison tests after two-way or repeated-measures ANOVA. *P* values of <0.05 were considered statistically significant.

RESULTS

Antibiotic Treatment Significantly Reduced Gut Microbiota Abundance and Affected Systemic Glucose Metabolism in Mice

To determine the effect of gut microbiome depletion on renal glucose metabolism, mice received ABX consisting of ampicillin, vancomycin, and levofloxacin in drinking water. After ABX treatment for 14 days, the expression level of bacterial 16s rRNA and the amount of SCFAs and bile acid in the colon or intestinal luminal contents were quantified. Luminal 16s rRNA expression, acetate, propionate, butyrate, cholate, deoxycholate, and ursodeoxycholate levels of ABX-treated mice were significantly lower than those of the control group (vehicle treated; Fig. 1, *A–D*); this indicated that ABX treatment effectively induced commensal depletion.

ABX-treated mice had a significantly lower body weight than vehicle-treated mice (Fig. 1*E*). No significant change was observed in plasma SCFA concentrations (Fig. 1*F*). ABX treatment significantly increased the plasma GLP-1 level (Fig. 1*G*) but did not affect the insulin level (Fig. 1*H*). An intraperitoneal glucose injection after 4 h of fasting revealed that the total area under the plasma glucose concentration curve (AUC) and AUC above baseline (incremental AUC) in ABX-treated mice were significantly lower than those in vehicle-treated mice (Fig. 1, *I–K*). These results suggest that AIMD was successfully induced by the ampicillin, vancomycin, and levofloxacin cocktail, consequently altering systemic glucose metabolism in mice.

ABX Treatment Significantly Altered Renal Glucose Metabolism in Mice

After ABX treatment for 14 days, renal glucose and pyruvate concentrations in ABX-treated mice were significantly lower than those in vehicle-treated mice (Fig. 2, *A–C*). We hypothesized that these changes in tissue concentrations of glucose and pyruvate could subsequently alter glucose homeostasis in the kidney.

To confirm whether AIMD altered glucose metabolism in the kidney, changes in whole body glucose metabolism were time dependently examined on *days 3*, *7*, *10*, or *14* of ABX treatment (Fig. 3). During *days 3–14*, significant differences were observed in colonic 16s rRNA expression levels and plasma GLP-1 concentrations between ABX- and vehicle-treated mice (Fig. 3, *A* and *B*). Compared with the control, plasma and renal glucose levels were significantly decreased in ABX-treated mice during *days 7–14* (Fig. 3, *C* and *D*). No significant change was observed in plasma pyruvate concentrations (Fig. 3*E*); however, renal pyruvate concentrations were significantly decreased in ABX-treated mice on *days 10* and *14* (Fig. 3*F*). On the other hand, no changes occurred in plasma and renal lactate concentrations of ABX- and vehicle-treated mice during *days 3–14* (Fig. 3, *G* and *H*).

We then determined mRNA expression levels of *G6pc* and hexokinases in whole kidney samples using quantitative RT-PCR. The renal *G6pc* expression level was found to be significantly higher in ABX-treated mice than in vehicle-treated mice (Fig. 4*A*). Conversely, ABX treatment did not affect mRNA expression levels of *Hk1*, *Hk2*, and *Hk3*. To clarify whether AIMD contributed to the changes in renal gluconeogenesis, we further assessed mRNA expression levels of key genes and concentrations of intermediate metabolites of glucose metabolism in the renal cortex (Fig. 4, *B–J*). mRNA expression levels of *G6pc* and *Pepck* in the renal cortex were significantly higher in the ABX-treated group than in the vehicle-treated group (Fig. 4*B*). ABX treatment did not affect mRNA expression levels of *Glut1*, *Glut2*, *Sglt1*, *Sglt2*, *Hk1*, *Hk2*, *Hk3*, *Fbp1*, *Pcx*, *Ldha*, and *Ldhb*. Similar to whole kidney samples, significant decreases in glucose and pyruvate concentrations were observed in the renal cortex after 14 days of treatment with ABX (Fig. 4, *C* and *D*). In addition, the lactate concentration was significantly lower in ABX-treated mice than in vehicle-treated mice (Fig. 4*E*). Among the tricarboxylic acid cycle intermediates, the concentration of malate was significantly increased by ABX treatment (Fig. 4*J*). The effects of ABX on citrate, α-ketoglutarate, succinate, and fumarate were insignificant (Fig. 4, *F–I*).

ABX Treatment Significantly Altered Renal Glucose Metabolism in Mice After Ischemia

We found significant effects of renal ischemia on glucose, pyruvate, and lactate levels in the kidneys of vehicle-treated mice (Fig. 5, *A–C*). Likewise, we also observed that ABX treatment significantly reduced glucose and pyruvate concentrations in control kidney samples, which was consistent with the above-mentioned results (Figs. 2 and 3). Compared with

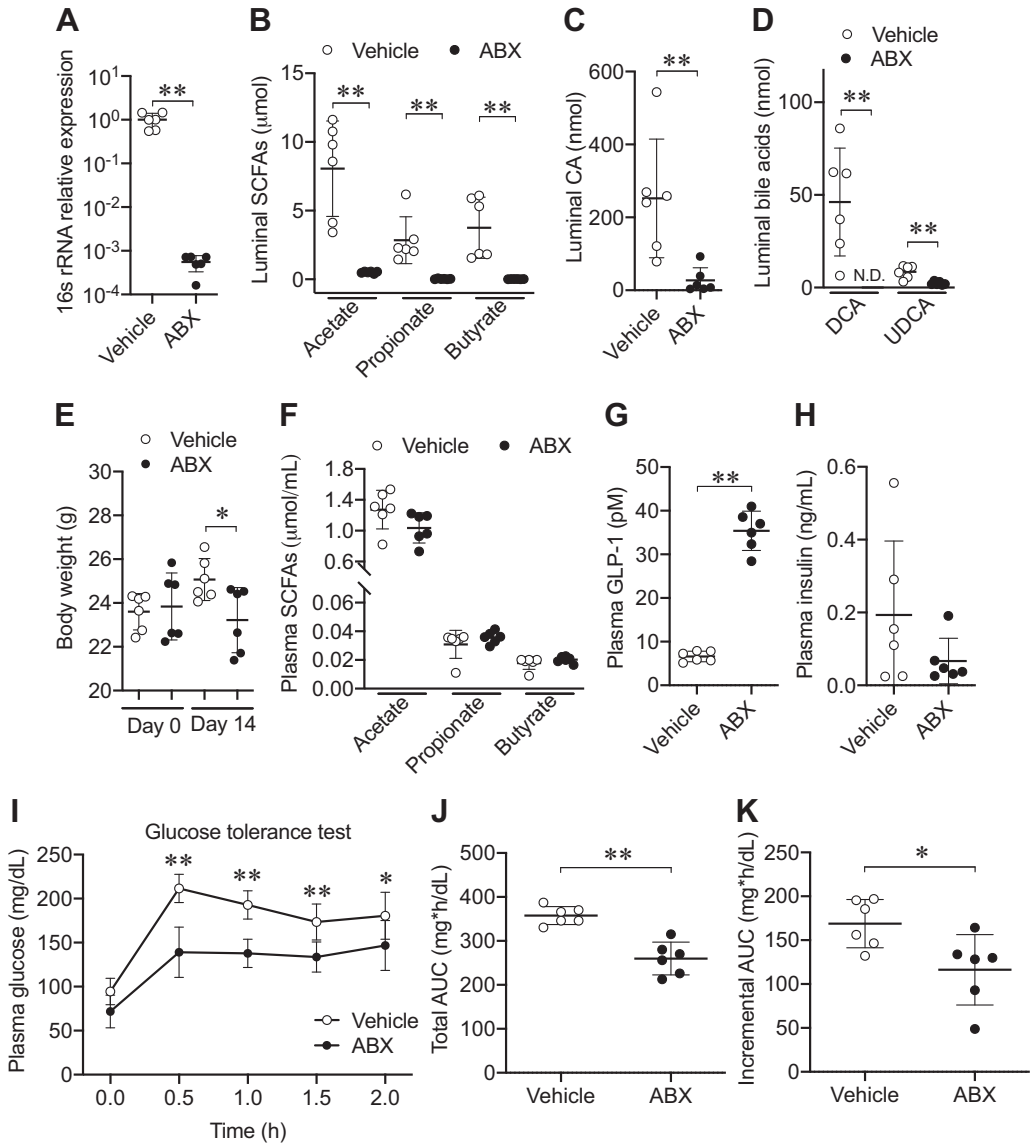

Figure 1. Altered glucose metabolism in antibiotic cocktail (ABX)-treated mice. For commensal depletion, ABX (1 g/L ampicillin, 0.5 g/L vancomycin, and 0.5 g/L levofloxacin) was administered to mice ($n = 6$) via drinking water for 14 days. The control group ($n = 6$) received vehicle (sterilized water) alone. *A–D*: efficacy of microbiome depletion assessed by determining expression levels of 16s rRNA (*A*) and amounts of short-chain fatty acids (SCFAs; *B*) and bile acids [cholate (CA), deoxycholate (DCA), and ursodeoxycholate (UDCA)] (*C* and *D*) in colonic luminal contents. *E–H*: effects of ABX treatment on body weight (*E*), plasma SCFAs (*F*), glucagon-like peptide 1 (GLP-1; *G*), and insulin (*H*) levels. *I–K*: a glucose tolerance test was performed in fasted mice after intraperitoneal injection with glucose. Based on plasma glucose levels, the total area under the concentration curve (total AUC; *J*) and AUC above baseline (incremental AUC; *K*) were calculated. Data are expressed as means ± SD. Statistical differences were evaluated using an unpaired *t* test (*A–D*, *F–H*, *J*, and *K*) or Bonferroni's multiple-comparison test (*E* and *I*). $^*P < 0.05$; $^{**}P < 0.01$.

vehicle-treated ischemic mice, pyruvate concentrations were significantly lower in ABX-treated ischemic mice (Fig. 5*B*). However, no significant difference was observed between control and ischemic kidney samples of ABX-treated mice (Fig. 5*B*). In addition, no changes were observed in renal glucose and lactate levels of ABX-treated ischemic mice (Fig. 5, *A* and *C*).

Since pyruvate can be converted to acetyl-CoA and ATP, we also quantified acetyl-CoA and ATP levels in control and ischemic kidney samples. Ischemia significantly reduced renal acetyl-CoA and ATP levels in both vehicle- and ABX-treated mice (Fig. 5, *D* and *E*). In contrast, ABX treatment did not affect acetyl-CoA concentrations in both control and ischemic kidney samples. On the other hand, ATP levels in control kidneys were significantly lower in ABX-treated mice than in vehicle-treated mice, whereas ATP levels were comparable between the ischemic kidneys of ABX- and vehicle-treated mice.

Given the cytoprotective role of pyruvate against IR injury (19), we also investigated the severity of renal IR injury in ABX-treated mice. The results showed that ABX treatment alone did not cause renal tubular injury (Fig. 6). Tubular injury associated with IR was prominent in the OSOM (Fig. 6, *A* and *D*). Tubular injury scores in the renal cortices and Kim-1-positive areas in the OSOM of ABX-treated mice were higher than those of vehicle-treated mice (Fig. 6, *B–D* and *F*).

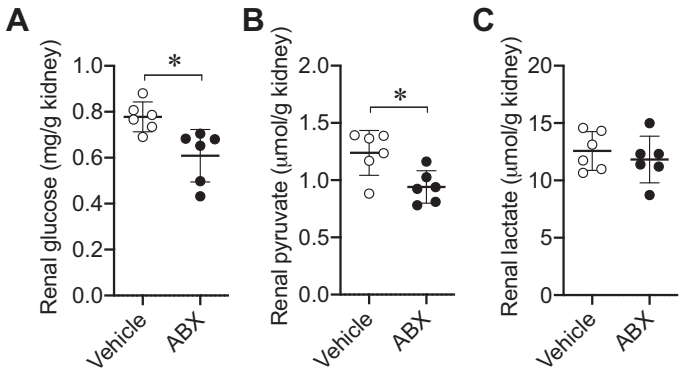

Figure 2. Antibiotic cocktail (ABX) treatment altered renal glucose metabolism in mice. *A*: glucose concentration in whole kidney homogenates quantified using a colorimetric assay. *B* and *C*: pyruvate and lactate concentrations in whole kidney homogenates quantified using liquid chromatography-tandem mass spectrometry. Data are expressed as means ± SD; $n = 6$ mice/group. Statistical differences were evaluated using an unpaired *t* test. $^*P < 0.05$.

DISCUSSION

Despite emerging evidence demonstrating the impact of AIMD on host metabolic homeostasis (10, 11, 22, 23, 42, 43), the effect of AIMD on renal glucose metabolism is yet to be elucidated. Hence, the present study addressed this concern by investigating the impact of AIMD on glucose metabolism in mouse kidneys and then observing the effect of ABX treatment on renal pyruvate levels after ischemia. Our findings suggested that ABX treatment significantly altered renal glucose metabolism in mice and was associated with more severe tubular injury following renal IR.

The results of this study indicated that AIMD altered renal glucose metabolism and pyruvate levels in mice. Significant effects of AIMD on glucose metabolism have also been observed in the intestine and liver (11, 23, 42), suggesting that AIMD can alter host systemic glucose metabolism. AIMD-induced decrease in renal pyruvate levels was possibly triggered by the inactivation of glycolysis, activation of gluconeogenesis, and facilitative conversion of pyruvate to acetyl-CoA or lactate (Fig. 4*K*). In the present study, ABX treatment upregulated *G6pc* and *Pepck* mRNA expression in the kidney but did not affect expression levels of other key genes involved in glucose metabolism. In addition, no significant changes in the plasma pyruvate concentration and renal acetyl-CoA levels were observed. Taken together, these findings suggest that AIMD enhances renal gluconeogenesis, leading to decreased pyruvate levels in the kidney.

We showed that AIMD not only triggered the upregulation of genes involved in gluconeogenesis in the kidney but also increased plasma levels of GLP-1, an incretin hormone with an inhibitory effect on gluconeogenesis. A previous study showed that loss of gut microbiota was accompanied by an increase in plasma levels of glucagon, and the increase in plasma GLP-1 and glucagon levels resulted from the upregulation of the proglucagon gene in the cecum and colon (11, 44). Glucagon has been known to regulate gene expression levels of *Pepck* and *G6pc* through activation of a transcription factor, forkhead box protein 1 (Foxo1) (45). Therefore, in AIMD mice, glucagon secreted from intestinal epithelial cells might act on renal proximal tubules, thereby affecting renal gluconeogenesis.

The SCFAs and bile acids produced by intestinal bacteria serve as nutrient sources for host intestinal epithelial cells. Therefore, when the supply of these metabolites is reduced

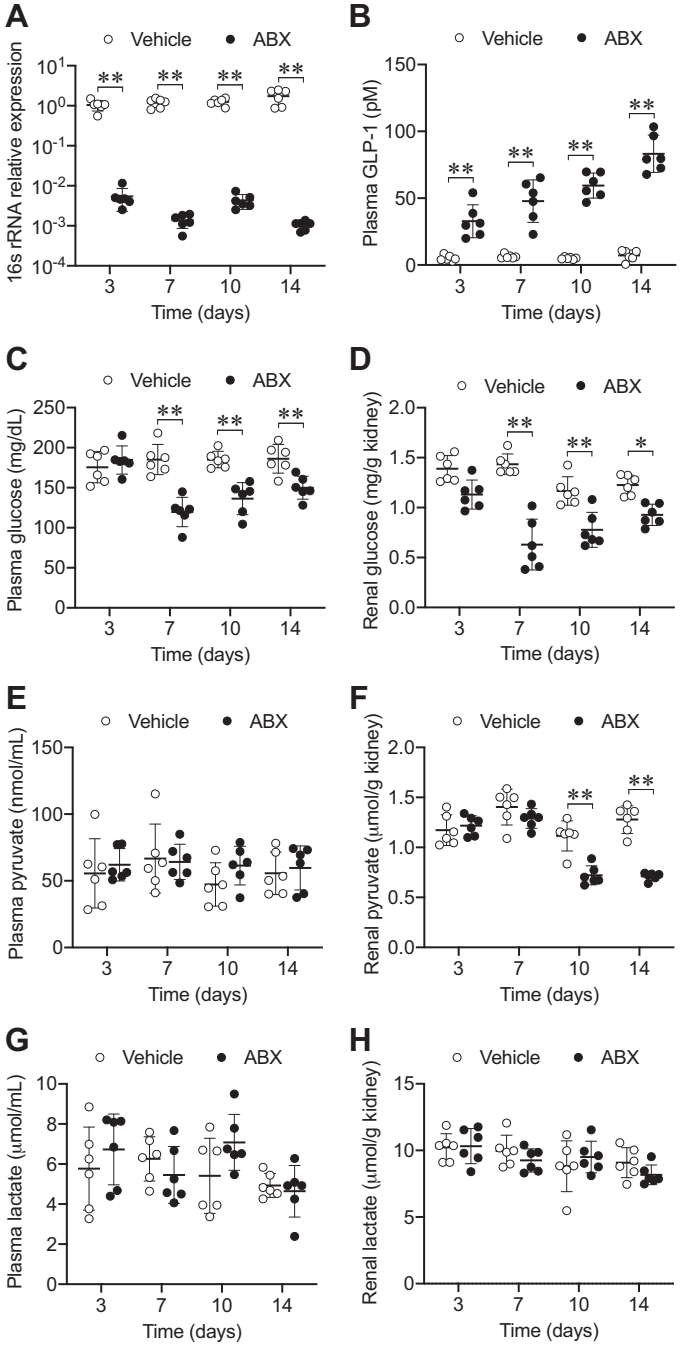

Figure 3. Time-dependent changes in renal glucose metabolism of antibiotic cocktail (ABX)-treated mice. The plasma, colon, and kidney were collected after treatment with ABX or vehicle on *days 3*, *7*, *10*, and *14*. The relative abundance of 16s rRNA in the colonic luminal contents (*A*) and levels of glucagon-like peptide 1 (GLP-1; *B*), glucose (*C* and *D*), pyruvate (*E* and *F*), and lactate (*G* and *H*) in the plasma or kidneys were quantified. Data are expressed as means ± SD; $n = 6$ mice/group. Statistical differences were evaluated using Tukey's multiple-comparison test. $^*P < 0.05$; $^{**}P < 0.01$.

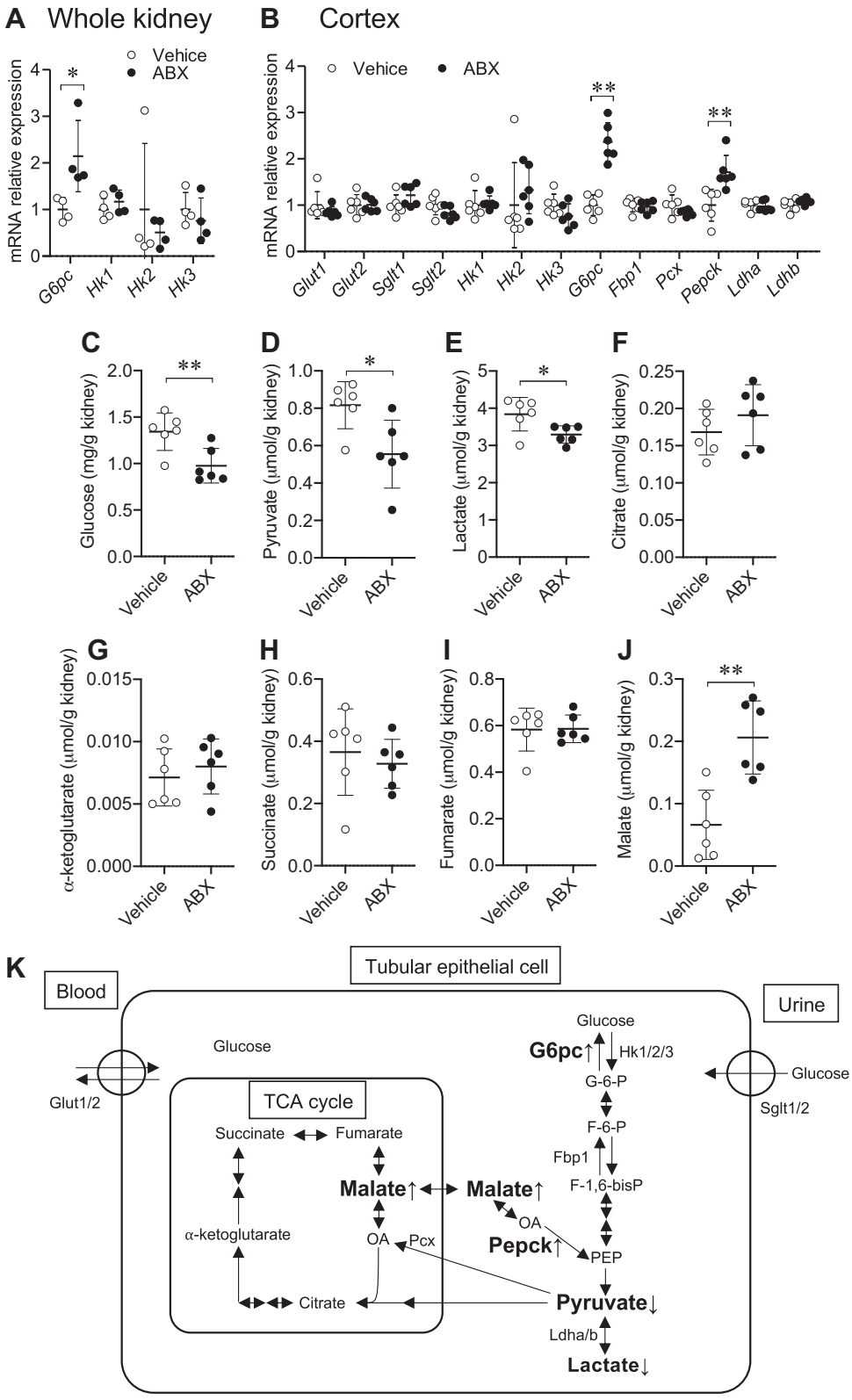

Figure 4. Antibiotic cocktail (ABX) treatment affected the gluconeogenic pathway in the kidney. *A*: relative mRNA expression levels of glucose-6-phosphatase (*G6pc*) and hexokinases [hexokinase 1 (*Hk1*), hexokinase 2 (*Hk2*), and hexokinase 3 (*Hk3*)] in whole kidney samples were determined using quantitative RT-PCR. *B*: relative mRNA expression levels of glucose transporter 1 (*Glut1*), glucose transporter 2 (*Glut2*), Na^+-glucose cotransporter 1 (*Sglt1*), Na^+-glucose cotransporter 2 (*Sglt2*), *Hk1*, *Hk2*, *Hk3, G6pc*, fructose-bisphosphatase 1 (*Fbp1*), pyruvate carboxylase (*Pcx*), phosphoenolpyruvate carboxykinase 1 (*Pepck*), lactate dehydrogenase A (*Ldha*), and lactate dehydrogenase B (*Ldhb*) in the renal cortex. *C–J*: concentrations of glucose and intermediate metabolites of glucose metabolism in the renal cortex. Data are expressed as means ± SD; $n = 4$ or 6 mice/group. Statistical differences were evaluated using an unpaired *t* test. $^*P < 0.05$; $^{**}P < 0.01$. *K*: antibiotic-induced microbiome depletion initiates metabolic reactions in the renal cortex. Bold font indicates genes or metabolites in which changes were observed after ABX treatment. F-1,6,-bisP, fructose-1,6-bisphosphate; F-6-P, fructose-6-phosphate; G-6-P, glucose-6-phosphate; OA, oxaloacetate; PEP, phosphoenolpyruvate; TCA, tricarboxylic acid.

by ABX treatment, the primary energy source for enterocytes may change, triggering increased glucose utilization (11). Contrariwise, we found that ABX-induced loss of colonic SCFAs did not affect plasma SCFA concentrations. In vehicle-treated mice, colon concentrations of SCFAs were 10–100 times higher than the plasma concentration. Therefore, we reasoned that most SCFAs produced in the gastrointestinal tract are consumed by intestinal epithelial

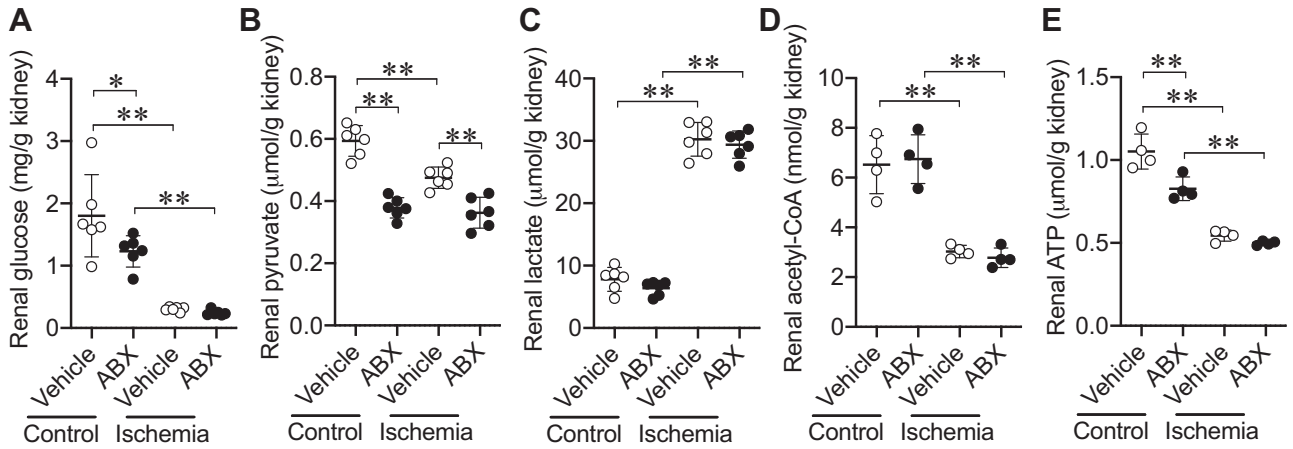

Figure 5. Antibiotic cocktail (ABX) treatment reduced renal pyruvate levels during ischemia. After 14 days of treatment with ABX or vehicle, mice were subjected to unilateral renal pedicle clamping (ischemia model) for 60 min, with the contralateral kidney as the control. Levels of glucose (*A*), pyruvate (*B*), lactate (*C*), acetyl-CoA (*D*), and ATP (*E*) in whole kidney samples were determined. Data are expressed as means ± SD; $n = 4$ or 6 mice/group. Statistical differences were evaluated using an unpaired *t* test. $^{*}P < 0.05$; $^{**}P < 0.01$.

cells and hepatocytes and that the contribution of microbiota-derived SCFAs to the amount of circulating SCFAs in mice is low.

Antibiotics are commonly prescribed in general medical practice, and nephrotoxic antibiotics, such as aminoglycosides (46) and glycopeptides (47), are believed to cause AKI (48, 49). However, the mechanisms underlying antibiotic-associated AKI are not fully understood. The present results suggested that ABX treatment increased the vulnerability of kidneys to IR injury. This concept may be supported by recent studies where the effect of microbiome depletion or dysbiosis on renal IR injury was examined (50, 51). In these previous studies, researchers indicated that the antibiotic-induced changes in gut microbiome composition could be associated with the development of kidney injury and that germ-free mice exhibited an increase in injury grading scales of tubular necrosis following renal IR (16, 29). In addition, we found that ABX treatment significantly altered renal pyruvate levels in both control and ischemic kidneys. Pyruvate not only acts as an intermediate in glucose metabolism to produce ATP but also exerts cytoprotective effects against tissue injury in the kidney (52), liver (53), heart (54), and brain (55, 56). Therefore, the adverse effects of microbiome depletion on the kidneys might be due to the reduced renal pyruvate levels. Alternatively, Yang et al. (57) reported that oral administration of four broad-spectrum antibiotics (ampicillin, metronidazole, neomycin, and vancomycin) ameliorated tubular necrosis following IR injury in mice, and they suggested that this renoprotective effect is partly mediated by the reduction of T helper cell 17 and T helper cell 1 responses, expansion of regulatory T cells, and M2 macrophages. Similarly, a study by Emal et al. (58) demonstrated that concomitant administration of antibiotics (ampicillin, metronidazole, neomycin, and vancomycin) with glucose protects the proximal tubules against IR injury, suggesting that antibiotic treatment may have affected the maturation of renal resident macrophages and bone marrow-derived monocytes. However, in the latter two studies, the degree of microbiome depletion, plasma glucose levels, and renal pyruvate levels were not evaluated. Thus, combined with our results and previous studies, the degree of gut microbiome depletion or renal pyruvate reduction may help determine the prognosis of the kidney following renal IR injury. However, further studies are warranted to fully elucidate this concept.

Given the large number of patients using antibiotics, it is important to understand the effect of antibiotics on renal physiology. The results of the present study suggest that antibiotic use may cause renal metabolic remodeling. Nonetheless, there are several limitations in the present study. First, we used ABX to eliminate gut bacteria. Second, we only focused on glucose metabolism; therefore, future studies are required to examine the effect of a single antibiotic class on global metabolic changes in the kidney. Third, our results could not provide cell- or organelle-specific insights. However, proximal tubular epithelial cells have a substantial capacity for gluconeogenesis (59, 60), with the proximal tubular mass constituting more than 50% of normal kidney volume (61); thus, the observed metabolic alterations reflected, at least in part, physiological changes in proximal tubules.

In conclusion, our data highlight the significant impact of AIMD on renal glucose metabolism in mice. Furthermore, this is the first report, to our knowledge, confirming that AIMD is associated with decreased levels of pyruvate, a key intermediate in glucose metabolism, which may have been caused by renal gluconeogenesis activation. Therefore, we hypothesize that AIMD can increase the susceptibility of kidneys to IR injury, which may be associated with the reduced renal pyruvate concentrations observed following ABX treatment.

Perspectives and Significance

We found that AIMD in mice was associated with pyruvate reduction and upregulation of *G6pc* and *Pepck* in the renal cortex. These results suggest that AIMD enhances renal gluconeogenesis and further gives the perspective that antibiotic use may cause renal metabolic remodeling. Future studies are required to examine the effect of a single antibiotic class on global metabolic changes in the kidney. In

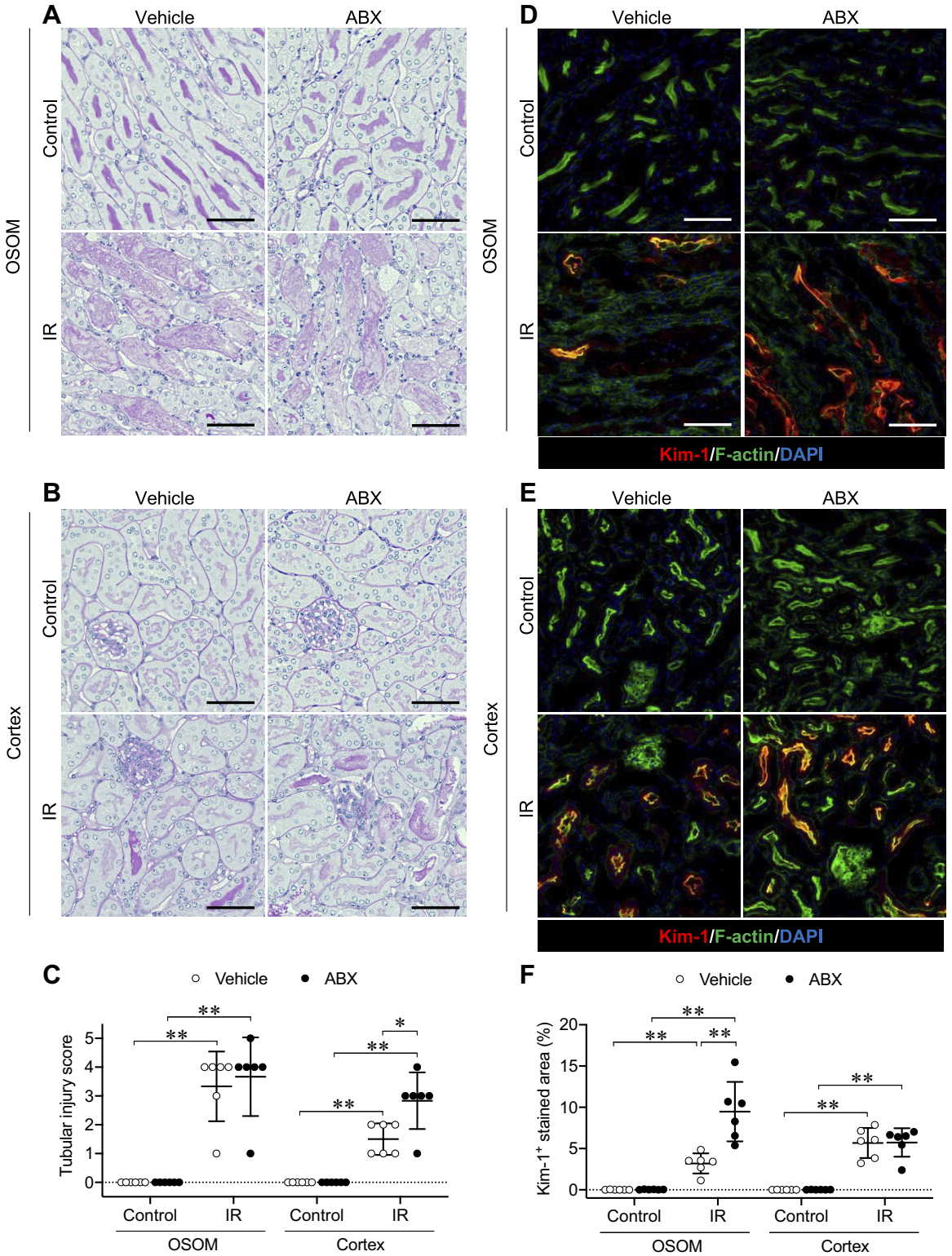

Figure 6. Antibiotic cocktail (ABX) treatment affected the severity of renal ischemia-reperfusion (IR) injury. After 14 days of treatment with ABX or vehicle, the left renal pedicle was clamped for 30 min and followed by 24-h reperfusion. Subsequently, the contralateral (control) and ipsilateral (IR) kidneys were resected. *A–C*: representative photographs of periodic acid-Schiff (PAS) staining. OSOM, outer stripe of the outer medulla. Magnification: ×200. Scale bars = 100 μm. Tubular injury in the OSOM and cortex were scored semiquantitatively using a scale of 0–5 (where 0 = no tubular injury, 1 = ≤10% tubules injured, 2 = 10–25% tubules injured, 3 = 25–50% tubules injured, 4 = 50–75% tubules injured, and 5 = ≥75% tubules injured). Tubular injury was defined as tubular necrosis, tubular cast formation, and loss of the brush border. *D–F*: mouse kidney sections stained with an antibody against kidney injury molecule-1 (Kim-1). The red signals for Kim-1 were merged with green signals for F-actin (phalloidin) and blue signals for 4′,6-diamidino-2-phenylindole (DAPI) in the same section. Magnification: ×200. Scale bars = 100 μm. The stained area in each section was quantified and presented as a percentage of the total area. Data are expressed as means ± SD; $n = 6$ mice/group. Statistical differences were evaluated using Tukey's multiple-comparison test. *$P < 0.05$; **$P < 0.01$.

addition, the present results suggested that antibiotic treatment increased the vulnerability of kidneys to IR injury. The degree of gut microbiome depletion or renal pyruvate reduction may help determine the prognosis of the kidney following renal IR injury. However, further studies are warranted to fully elucidate this concept.

GRANTS

This work was supported in part by Grants-in-Aid for Scientific Research (KAKENHI) from the Ministry of Education, Science, Culture, and Sports of Japan or the Japanese Society for the Promotion of Science [Grants-in-Aid for Scientific Research [C] to S. Nakagawa (18K06783)].

DISCLOSURES

No conflicts of interest, financial or otherwise, are declared by the authors.

AUTHOR CONTRIBUTIONS

Y.O., S.N., and K.M. conceived and designed research; Y.O., K. Ishibe., S.T., and A.S. performed experiments; S.N. and K. Itohara analyzed data; Y.O., K.M., S.N., S.I., A.Y., and T.N. interpreted results of experiments; Y.O., S.N., T.N., and K.M. prepared figures; Y.O., S.N., K. Ishibe, T.N., and K.M. drafted manuscript; S.N., S.I., A.Y., and K.M. edited and revised manuscript; Y.O., S.N., K. Ishibe, S.T., A.S., K. Itohara., S.I., A.Y., T.N., and K.M. approved final version of manuscript.

REFERENCES

1. **Tulstrup MV**, **Christensen EG**, **Carvalho V**, **Linninge C**, **Ahrné S**, **Højberg O**, **Licht TR**, **Bahl MI.** Antibiotic treatment affects intestinal permeability and gut microbial composition in Wistar rats dependent on antibiotic class. *PLoS One* 10: e0144854, 2015. doi:10.1371/journal.pone.0144854.
2. **Zimmermann P**, **Curtis N.** The effect of antibiotics on the composition of the intestinal microbiota - a systematic review. *J Infect* 79: 471–489, 2019. doi:10.1016/j.jinf.2019.10.008.
3. **Rogers MB**, **Firek B**, **Shi M**, **Yeh A**, **Brower-Sinning R**, **Aveson V**, **Kohl BL**, **Fabio A**, **Carcillo JA**, **Morowitz MJ.** Disruption of the microbiota across multiple body sites in critically ill children. *Microbiome* 4: 66, 2016. doi:10.1186/s40168-016-0211-0.
4. **Vincent JL**, **Rello J**, **Marshall J**, **Silva E**, **Anzueto A**, **Martin CD**, **Moreno R**, **Lipman J**, **Gomersall C**, **Sakr Y**, **Reinhart K**; **EPIC II Group of Investigators.** International study of the prevalence and outcomes of infection in intensive care units. *JAMA* 302: 2323–2329, 2009. doi:10.1001/jama.2009.1754.
5. **Wolff NS**, **Hugenholtz F**, **Wiersinga WJ.** The emerging role of the microbiota in the ICU. *Crit Care* 22: 78, 2018. doi:10.1186/s13054-018-1999-8.
6. **Becattini S**, **Taur Y**, **Pamer EG.** Antibiotic-induced changes in the intestinal microbiota and disease. *Trends Mol Med* 22: 458–478, 2016. doi:10.1016/j.molmed.2016.04.003.
7. **Reijnders D**, **Goossens GH**, **Hermes GD**, **Neis EP**, **van der Beek CM**, **Most J**, **Holst JJ**, **Lenaerts K**, **Kootte RS**, **Nieuwdorp M**, **Groen AK**, **Olde Damink SW**, **Boekschoten MV**, **Smidt H**, **Zoetendal EG**, **Dejong CH**, **Blaak EE.** Effects of gut microbiota manipulation by antibiotics on host metabolism in obese humans: a randomized double-blind placebo-controlled trial. *Cell Metab* 24: 63–74, 2016. doi:10.1016/j.cmet.2016.06.016.
8. **Baumgartner S**, **Reijnders D**, **Konings MCJM**, **Groen AK**, **Lütjohann D**, **Goossens GH**, **Blaak EE**, **Plat J.** The effects of amoxicillin and vancomycin on parameters reflecting cholesterol metabolism. *Chem Phys Lipids* 207: 239–245, 2017. doi:10.1016/j.chemphyslip.2017.06.006.
9. **Behr C**, **Sperber S**, **Jiang X**, **Strauss V**, **Kamp H**, **Walk T**, **Herold M**, **Beekmann K**, **Rietjens IMCM**, **van Ravenzwaay B.** Microbiome-related metabolite changes in gut tissue, cecum content and feces of rats treated with antibiotics. *Toxicol Appl Pharmacol* 355: 198–210, 2018. doi:10.1016/j.taap.2018.06.028.
10. **Martin AM**, **Yabut JM**, **Choo JM**, **Page AJ**, **Sun EW**, **Jessup CF**, **Wesselingh SL**, **Khan WI**, **Rogers GB**, **Steinberg GR**, **Keating DJ.** The gut microbiome regulates host glucose homeostasis via peripheral serotonin. *Proc Natl Acad Sci USA* 116: 19802–19804, 2019. doi:10.1073/pnas.1909311116.
11. **Zarrinpar A**, **Chaix A**, **Xu ZZ**, **Chang MW**, **Marotz CA**, **Saghatelian A**, **Knight R**, **Panda S.** Antibiotic-induced microbiome depletion alters metabolic homeostasis by affecting gut signaling and colonic metabolism. *Nat Commun* 9: 2872, 2018. doi:10.1038/s41467-018-05336-9.
12. **Mather A**, **Pollock C.** Glucose handling by the kidney. *Kidney Int* 79 *Suppl* 120: S1–S6, 2011. doi:10.1038/ki.2010.509.
13. **Gerich JE**, **Meyer C**, **Woerle HJ**, **Stumvoll M.** Renal gluconeogenesis: its importance in human glucose homeostasis. *Diabetes Care* 24: 382–391, 2001. doi:10.2337/diacare.24.2.382.
14. **Jang C**, **Hui S**, **Zeng X**, **Cowan AJ**, **Wang L**, **Chen L**, **Morscher RJ**, **Reyes J**, **Frezza C**, **Hwang HY**, **Imai A**, **Saito Y**, **Okamoto K**, **Vaspoli C**, **Kasprenski L**, **Zsido GA**, **Gorman JH**, **Gorman RC**, **Rabinowitz JD.** Metabolite exchange between mammalian organs quantified in pigs. *Cell Metab* 30: 594–606.e3, 2019. doi:10.1016/j.cmet.2019.06.002.
15. **Owen OE**, **Felig P**, **Morgan AP**, **Wahren J**, **Cahill GF.** Liver and kidney metabolism during prolonged starvation. *J Clin Invest* 48: 574–583, 1969. doi:10.1172/JCI106016.
16. **Maitra SR**, **Homan CS**, **Pan W**, **Geller ER**, **Henry MC**, **Thode HC.** Renal gluconeogenesis and blood flow during endotoxic shock. *Acad Emerg Med* 3: 1006–1010, 1996. doi:10.1111/j.1553-2712.1996.tb03343.x.
17. **Meyer C**, **Stumvoll M**, **Nadkarni V**, **Dostou J**, **Mitrakou A**, **Gerich J.** Abnormal renal and hepatic glucose metabolism in type 2 diabetes mellitus. *J Clin Invest* 102: 619–624, 1998. doi:10.1172/JCI2415.
18. **Legouis D**, **Ricksten SE**, **Faivre A**, **Verissimo T**, **Gariani K**, **Verney C**, **Galichon P**, **Berchtold L**, **Feraille E**, **Fernandez M**, **Placier S**, **Koppitch K**, **Hertig A**, **Martin PY**, **Naesens M**, **Pugin J**, **McMahon AP**, **Cippà PE**, **de Seigneux S.** Altered proximal tubular cell glucose metabolism during acute kidney injury is associated with mortality. *Nat Metab* 2: 732–743, 2020 [Erratum in *Nat Metab* 2: 989, 2020]. doi:10.1038/s42255-020-0238-1.
19. **Zager RA**, **Johnson AC**, **Becker K.** Renal cortical pyruvate depletion during AKI. *J Am Soc Nephrol* 25: 998–1012, 2014. doi:10.1681/ASN.2013070791.
20. **Smith JA**, **Stallons LJ**, **Schnellmann RG.** Renal cortical hexokinase and pentose phosphate pathway activation through the EGFR/Akt signaling pathway in endotoxin-induced acute kidney injury. *Am J Physiol Renal Physiol* 307: F435–F444, 2014. doi:10.1152/ajprenal.00271.2014.
21. **Rodrigues RR**, **Greer RL**, **Dong X**, **DSouza KN**, **Gurung M**, **Wu JY**, **Morgun A**, **Shulzhenko N.** Antibiotic-induced alterations in gut microbiota are associated with changes in glucose metabolism in healthy mice. *Front Microbiol* 8: 2306, 2017. doi:10.3389/fmicb.2017.02306.
22. **Li B**, **Li L**, **Li M**, **Lam SM**, **Wang G**, **Wu Y**, **Zhang H**, **Niu C**, **Zhang X**, **Liu X**, **Hambly C**, **Jin W**, **Shui G**, **Speakman JR.** Microbiota depletion impairs thermogenesis of brown adipose tissue and browning of white adipose tissue. *Cell Rep* 26: 2720–2737.e5, 2019. doi:10.1016/j.celrep.2019.02.015.
23. **Krisko TI**, **Nicholls HT**, **Bare CJ**, **Holman CD**, **Putzel GG**, **Jansen RS**, **Sun N**, **Rhee KY**, **Banks AS**, **Cohen DE.** Dissociation of adaptive thermogenesis from glucose homeostasis in microbiome-deficient mice. *Cell Metab* 31: 592–604.e9, 2020. doi:10.1016/j.cmet.2020.01.012.
24. **Fujisaka S**, **Ussar S**, **Clish C**, **Devkota S**, **Dreyfuss JM**, **Sakaguchi M**, **Soto M**, **Konishi M**, **Softic S**, **Altindis E**, **Li N**, **Gerber G**, **Bry L**, **Kahn CR.** Antibiotic effects on gut microbiota and metabolism are host dependent. *J Clin Invest* 126: 4430–4443, 2016. doi:10.1172/JCI86674.
25. **Nakanishi Y**, **Sato T**, **Ohteki T.** Commensal gram-positive bacteria initiates colitis by inducing monocyte/macrophage mobilization. *Mucosal Immunol* 8: 152–160, 2015. doi:10.1038/mi.2014.53.
26. **Han J**, **Gagnon S**, **Eckle T**, **Borchers CH.** Metabolomic analysis of key central carbon metabolism carboxylic acids as their 3-nitrophenylhydrazones by UPLC/ESI-MS. *Electrophoresis* 34: 2891–2900, 2013. doi:10.1002/elps.201200601.
27. **Han J**, **Lin K**, **Sequeira C**, **Borchers CH.** An isotope-labeled chemical derivatization method for the quantitation of short-chain fatty acids

in human feces by liquid chromatography-tandem mass spectrometry. *Anal Chim Acta* 854: 86–94, 2015. doi:10.1016/j.aca.2014.11.015.
28. **Jin YY**, **Shi ZQ**, **Chang WQ**, **Guo LX**, **Zhou JL**, **Liu JQ**, **Liu LF**, **Xin GZ.** A chemical derivatization based UHPLC-LTQ-Orbitrap mass spectrometry method for accurate quantification of short-chain fatty acids in bronchoalveolar lavage fluid of asthma mice. *J Pharm Biomed Anal* 161: 336–343, 2018. doi:10.1016/j.jpba.2018.08.057.
29. **Chen Z**, **Gao Z**, **Wu Y**, **Shrestha R**, **Imai H**, **Uemura N**, **Hirano KI**, **Chiba H**, **Hui SP.** Development of a simultaneous quantitation for short-, medium-, long-, and very long-chain fatty acids in human plasma by 2-nitrophenylhydrazine-derivatization and liquid chromatography-tandem mass spectrometry. *J Chromatogr B Analyt Technol Biomed Life Sci* 1126-1127: 121771, 2019. doi:10.1016/j.jchromb.2019.121771.
30. **Fu X**, **Deja S**, **Kucejova B**, **Duarte JAG**, **McDonald JG**, **Burgess SC.** Targeted determination of tissue energy status by lc-ms/ms. *Anal Chem* 91: 5881–5887, 2019. doi:10.1021/acs.analchem.9b00217.
31. **Masumoto S**, **Akimoto Y**, **Oike H**, **Kobori M.** Dietary phloridzin reduces blood glucose levels and reverses Sglt1 expression in the small intestine in streptozotocin-induced diabetic mice. *J Agric Food Chem* 57: 4651–4656, 2009. doi:10.1021/jf9008197.
32. **Hu J**, **Wang J**, **Li C**, **Shang Y.** Fructose-1,6-bisphosphatase aggravates oxidative stress-induced apoptosis in asthma by suppressing the Nrf_2 pathway. *J Cell Mol Med* 25: 5001–5014, 2021. doi:10.1111/jcmm.16439.
33. **Teshigawara K**, **Ogawa W**, **Mori T**, **Matsuki Y**, **Watanabe E**, **Hiramatsu R**, **Inoue H**, **Miyake K**, **Sakaue H**, **Kasuga M.** Role of Krüppel-like factor 15 in PEPCK gene expression in the liver. *Biochem Biophys Res Commun* 327: 920–926, 2005. doi:10.1016/j.bbrc.2004.12.096.
34. **Kang M**, **Lee SM**, **Kim W**, **Lee KH**, **Kim DY.** Fubp1 supports the lactate-Akt-mTOR axis through the upregulation of Hk1 and Hk2. *Biochem Biophys Res Commun* 512: 93–99, 2019. doi:10.1016/j.bbrc.2019.03.005.
35. **Nishihara K**, **Masuda S**, **Nakagawa S**, **Yonezawa A**, **Ichimura T**, **Bonventre JV**, **Inui K.** Impact of cyclin B2 and cell division cycle 2 on tubular hyperplasia in progressive chronic renal failure rats. *Am J Physiol Renal Physiol* 298: F923–F934, 2010. doi:10.1152/ajprenal.00567.2009.
36. **Zarjou A**, **Kim J**, **Traylor AM**, **Sanders PW**, **Balla J**, **Agarwal A**, **Curtis LM.** Paracrine effects of mesenchymal stem cells in cisplatin-induced renal injury require heme oxygenase-1. *Am J Physiol Renal Physiol* 300: F254–F262, 2011. doi:10.1152/ajprenal.00594.2010.
37. **Wei J**, **Song J**, **Jiang S**, **Zhang G**, **Wheeler D**, **Zhang J**, **Wang S**, **Lai EY**, **Wang L**, **Buggs J**, **Liu R.** Role of intratubular pressure during the ischemic phase in acute kidney injury. *Am J Physiol Renal Physiol* 312: F1158–F1165, 2017. doi:10.1152/ajprenal.00527.2016.
38. **Takaori K**, **Nakamura J**, **Yamamoto S**, **Nakata H**, **Sato Y**, **Takase M**, **Nameta M**, **Yamamoto T**, **Economides AN**, **Kohno K**, **Haga H**, **Sharma K**, **Yanagita M.** Severity and frequency of proximal tubule injury determines renal prognosis. *J Am Soc Nephrol* 27: 2393–2406, 2016. doi:10.1681/ASN.2015060647.
39. **Nakagawa S**, **Masuda S**, **Nishihara K**, **Inui K.** mTOR inhibitor everolimus ameliorates progressive tubular dysfunction in chronic renal failure rats. *Biochem Pharmacol* 79: 67–76, 2010. doi:10.1016/j.bcp.2009.07.015.
40. **Arai S**, **Kitada K**, **Yamazaki T**, **Takai R**, **Zhang X**, **Tsugawa Y**, **Sugisawa R**, **Matsumoto A**, **Mori M**, **Yoshihara Y**, **Doi K**, **Maehara N**, **Kusunoki S**, **Takahata A**, **Noiri E**, **Suzuki Y**, **Yahagi N**, **Nishiyama A**, **Gunaratnam L**, **Takano T**, **Miyazaki T.** Apoptosis inhibitor of macrophage protein enhances intraluminal debris clearance and ameliorates acute kidney injury in mice. *Nat Med* 22: 183–193, 2016. doi:10.1038/nm.4012.
41. **Bank JR**, **van der Pol P**, **Vreeken D**, **Monge-Chaubo C**, **Bajema IM**, **Schlagwein N**, **van Gijlswijk DJ**, **van der Kooij SW**, **Reinders MEJ**, **de Fijter JW**, **van Kooten C.** Kidney injury molecule-1 staining in renal allograft biopsies 10 days after transplantation is inversely correlated with functioning proximal tubular epithelial cells. *Nephrol Dial Transplant* 32: 2132–2141, 2017. doi:10.1093/ndt/gfx286.
42. **Li G**, **Xie C**, **Lu S**, **Nichols RG**, **Tian Y**, **Li L**, **Patel D**, **Ma Y**, **Brocker CN**, **Yan T**, **Krausz KW**, **Xiang R**, **Gavrilova O**, **Patterson AD**, **Gonzalez FJ.** Intermittent fasting promotes white adipose browning and decreases obesity by shaping the gut microbiota. *Cell Metab* 26: 801, 2017. doi:10.1016/j.cmet.2017.10.007.
43. **Nay K**, **Jollet M**, **Goustard B**, **Baati N**, **Vernus B**, **Pontones M**, **Lefeuvre-Orfila L**, **Bendavid C**, **Rué O**, **Mariadassou M**, **Bonnieu A**, **Ollendorff V**, **Lepage P**, **Derbré F**, **Koechlin-Ramonatxo C.** Gut bacteria are critical for optimal muscle function: a potential link with glucose homeostasis. *Am J Physiol Endocrinol Metab* 317: E158–E171, 2019. doi:10.1152/ajpendo.00521.2018.
44. **Wichmann A**, **Allahyar A**, **Greiner TU**, **Plovier H**, **Lundén G**, **Larsson T**, **Drucker DJ**, **Delzenne NM**, **Cani PD**, **Bäckhed F.** Microbial modulation of energy availability in the colon regulates intestinal transit. *Cell Host Microbe* 14: 582–590, 2013. doi:10.1016/j.chom.2013.09.012.
45. **Oh K-J**, **Han H-S**, **Kim M-J**, **Koo S-H.** CREB and FoxO1: two transcription factors for the regulation of hepatic gluconeogenesis. *BMB Rep* 46: 567–574, 2013. doi:10.5483/bmbrep.2013.46.12.248.
46. **Bellomo R**, **Kellum JA**, **Ronco C.** Acute kidney injury. *Lancet* 380: 756–766, 2012. doi:10.1016/S0140-6736(11)61454-2.
47. **Naughton CA.** Drug-induced nephrotoxicity. *Am Fam Physician* 78: 743–750, 2008.
48. **Muriithi AK**, **Leung N**, **Valeri AM**, **Cornell LD**, **Sethi S**, **Fidler ME**, **Sh N.** Biopsy-proven acute interstitial nephritis, 1993–2011: a case series. *Am J Kidney Dis* 64: 558–566, 2014. doi:10.1053/j.ajkd.2014.04.027.
49. **Rennie TJW**, **De Souza N**, **Donnan PT**, **Marwick CA**, **Davey P**, **Dreischulte T**, **Bell S.** Risk of acute kidney injury following community prescription of antibiotics: self-controlled case series. *Nephrol Dial Transplant* 34: 1910–1916, 2019. doi:10.1093/ndt/gfy187.
50. **Jang HR**, **Gandolfo MT**, **Ko GJ**, **Satpute S**, **Racusen L**, **Rabb H.** Early exposure to germs modifies kidney damage and inflammation after experimental ischemia-reperfusion injury. *Am J Physiol Renal Physiol* 297: F1457–F1465, 2009. doi:10.1152/ajprenal.90769.2008.
51. **Nakade Y**, **Iwata Y**, **Furuichi K**, **Mita M**, **Hamase K**, **Konno R**, **Miyake T**, **Sakai N**, **Kitajima S**, **Toyama T**, **Shinozaki Y**, **Sagara A**, **Miyagawa T**, **Hara A**, **Shimizu M**, **Kamikawa Y**, **Sato K**, **Oshima M**, **Yoneda-Nakagawa S**, **Yamamura Y**, **Kaneko S**, **Miyamoto T**, **Katane M**, **Homma H**, **Morita H**, **Suda W**, **Hattori M**, **Wada T.** Gut microbiota-derived D-serine protects against acute kidney injury. *JCI Insight* 3: e97957, 2018. doi:10.1172/jci.insight.97957.
52. **Johnson AC**, **Zager RA.** Renal cortical pyruvate as a potentially critical mediator of acute kidney injury. *Nephron Clin Pract* 127: 129–132, 2014. doi:10.1159/000363547.
53. **Sileri P**, **Schena S**, **Morini S**, **Rastellini C**, **Pham S**, **Benedetti E**, **Cicalese L.** Pyruvate inhibits hepatic ischemia-reperfusion injury in rats. *Transplantation* 72: 27–30, 2001. doi:10.1097/00007890-200107150-00008.
54. **DeBoer LW**, **Bekx PA**, **Han L**, **Steinke L.** Pyruvate enhances recovery of rat hearts after ischemia and reperfusion by preventing free radical generation. *Am J Physiol* 265: H1571–H1576, 1993. doi:10.1152/ajpheart.1993.265.5.H1571.
55. **Lee JY**, **Kim YH**, **Koh JY.** Protection by pyruvate against transient forebrain ischemia in rats. *J Neurosci* 21: RC171, 2001. doi:10.1523/JNEUROSCI.21-20-j0002.2001.
56. **Arya DS**, **Bansal P**, **Ojha SK**, **Nandave M**, **Mohanty I**, **Gupta SK.** Pyruvate provides cardioprotection in the experimental model of myocardial ischemic reperfusion injury. *Life Sci* 79: 38–44, 2006. doi:10.1016/j.lfs.2005.12.039.
57. **Yang J**, **Kim CJ**, **Go YS**, **Lee HY**, **Kim MG**, **Oh SW**, **Cho WY**, **Im SH**, **Jo SK.** Intestinal microbiota control acute kidney injury severity by immune modulation. *Kidney Int* 98: 932–946, 2020. doi:10.1016/j.kint.2020.04.048.
58. **Emal D**, **Rampanelli E**, **Stroo I**, **Butter LM**, **Teske GJ**, **Claessen N**, **Stokman G**, **Florquin S**, **Leemans JC**, **Dessing MC.** Depletion of gut microbiota protects against renal ischemia-reperfusion injury. *J Am Soc Nephrol* 28: 1450–1461, 2017. doi:10.1681/ASN.2016030255.
59. **Clar J**, **Gri B**, **Calderaro J**, **Birling MC**, **Hérault Y**, **Smit GP**, **Mithieux G**, **Rajas F.** Targeted deletion of kidney glucose-6 phosphatase leads to nephropathy. *Kidney Int* 86: 747–756, 2014. doi:10.1038/ki.2014.102.
60. **Eid A**, **Bodin S**, **Ferrier B**, **Delage H**, **Boghossian M**, **Martin M**, **Baverel G**, **Conjard A.** Intrinsic gluconeogenesis is enhanced in renal proximal tubules of Zucker diabetic fatty rats. *J Am Soc Nephrol* 17: 398–405, 2006. doi:10.1681/ASN.2005070742.
61. **Chevalier RL.** The proximal tubule is the primary target of injury and progression of kidney disease: role of the glomerulotubular junction. *Am J Physiol Renal Physiol* 311: F145–F161, 2016. doi:10.1152/ajprenal.00164.2016.